Modal properties and modal control in vertically emitting annular Bragg lasers

Xiankai Sun and Amnon Yariv

Department of Applied Physics, MC128-95, California Institute of Technology, Pasadena, CA 91125
xksun@caltech.edu

Abstract: The modal properties, including the resonant vertical radiation, of a type of laser structures based on the annular Bragg resonance (ABR) are studied in detail. The modal threshold gains and the resonance frequencies of such lasers are obtained from the derived governing characteristic equation. Two kinds of ABR lasers, one with a $\pi/2$ phase shift in the outer grating and the other without, are analyzed. It is numerically demonstrated that, it's possible to get a large-area, high-efficiency, single defect mode lasing in ABR lasers if we choose the kind without a $\pi/2$ phase shift in the outer grating and also a device size smaller than a critical value.

OCIS codes: (250.7270) Vertical emitting lasers; (230.1480) Bragg reflectors; (140.5960) Semiconductor lasers; (130.0130) Integrated optics.

References and links

1. T. Erdogan, and D. G. Hall, "Circularly symmetric distributed feedback semiconductor lasers: An analysis," J. Appl. Phys. **68**, 1435-1444 (1990).
2. C. Wu, M. Svilans, M. Fallahi, T. Makino, J. Glinski, C. Maritan, and C. Blaauw, "Optical Pumped Surface-Emitting DFB GaInAsP/InP Lasers with Circular Grating," Electron. Lett. **27**, 1819-1821 (1991).
3. T. Erdogan, O. King, G. W. Wicks, D. G. Hall, E. H. Anderson, and M. J. Rooks, "Circularly symmetric operation of a concentric-circle-grating, surface-emitting, AlGaAs/GaAs quantum-well semiconductor laser," Appl. Phys. Lett. **60**, 1921-1923 (1992).
4. C. Wu, M. Svilans, M. Fallahi, I. Templeton, T. Makino, J. Glinski, R. Maciejko, S. I. Najafi, C. Maritan, C. Blaauw, and G. Knight, "Room Temperature Operation of Electrically Pumped Surface-Emitting Circular Grating DBR Laser," Electron. Lett. **28**, 1037-1039 (1992).
5. C. Wu, T. Makino, S. I. Najafi, R. Maciejko, M. Svilans, J. Glinski, and M. Fallahi, "Threshold Gain and Threshold Current Analysis of Circular Grating DFB and DBR Lasers," IEEE J. Quantum Electron. **29**, 2596-2606 (1993).
6. A. M. Shams-Zadeh-Amiri, X. Li, and W. P. Huang, "Hankel transform-domain analysis of scattered fields in multilayer planar waveguides and lasers with circular gratings," IEEE J. Quantum Electron. **39**, 1086-1098 (2003).
7. R. H. Jordan, D. G. Hall, O. King, G. W. Wicks, and S. Rishton, "Lasing behavior of circular grating surface-emitting semiconductor lasers," J. Opt. Soc. Am. B **14**, 449-453 (1997).
8. J. Scheuer, and A. Yariv, "Coupled-Waves Approach to the Design and Analysis of Bragg and Photonic Crystal Annual Resonators," IEEE J. Quantum Electron. **39**, 1555-1562 (2003).
9. J. Scheuer, W. M. J. Green, G. DeRose, and A. Yariv, "Low-threshold two-dimensional annular Bragg lasers," Opt. Lett. **29**, 2641-2643 (2004).
10. X. K. Sun, J. Scheuer, and A. Yariv, "Optimal design and reduced threshold in vertically emitting circular Bragg disk resonator lasers," IEEE J. Sel. Top. Quantum Electron. **13**, 359-366 (2007).
11. A. Yariv, *Optical Electronics in Modern Communications* (Oxford Univ. Press, New York, 1997).
12. J. Scheuer, W. M. J. Green, G. A. DeRose, and A. Yariv, "InGaAsP Annular Bragg Lasers: Theory, Applications, and Modal Properties," IEEE J. Sel. Top. Quantum Electron. **11**, 476-484 (2005).
13. R. F. Kazarinov, and C. H. Henry, "Second-Order Distributed Feedback Lasers with Mode Selection Provided by First-Order Radiation Losses," IEEE J. Quantum Electron. **QE-21**, 144-150 (1985).

#87228 - $15.00 USD Received 5 Sep 2007; revised 1 Nov 2007; accepted 28 Nov 2007; published 10 Dec 2007

1. Introduction

Surface emitting lasers have been attracting people's interest over the past few years because of their salient features such as low threshold currents, single mode operation, and wafer-scale integration. Their low-divergence surface-normal emission also facilitates output coupling and packaging. Vertical Cavity Surface Emitting Lasers (VCSELs) have been commercially available since 2005. However, they can have a single transverse mode and a good emission pattern only for rather small mode areas (diameters of a few microns). For larger emission aperture, the excitation of higher-order transverse modes can not be avoided, which casts a shadow over the usefulness of VCSELs in high-power applications. On the other hand, circular-grating-coupled surface emitting lasers are promising candidates for high-power applications because of their broad and circular emission aperture and their potential in optical coherent combination in a 2-D laser array configuration. The optically and electrically pumped circular grating distributed feedback (DFB) and distributed Bragg reflector (DBR) lasers have been studied extensively [1-7]. Their radiation patterns have also been investigated theoretically [6] and verified experimentally [3, 7]. In those designs, people usually employ a grating periodic in the radial direction. This usually results in azimuthal modal degeneracy [1, 5], which makes it hard for mode selection.

In 2003, we proposed a novel type of circular resonator, referred to as "annular Bragg resonator (ABR)," which adopts chirped circular gratings rather than periodic circular gratings, for optimal light confinement in cylindrical geometry [8]. The designed defect mode has high emission efficiency. The demonstrated active devices based on these ABRs (i.e., annular Bragg lasers, or ABR lasers) have exhibited their superiority in low-threshold laser operation [9]. Nevertheless, they possessed multiple modes in the lasing spectra. The multi-mode behaviors cannot be analyzed in a passive model. Thus, a comprehensive coupled mode theory, including the effects of vertical radiation, has been developed and first applied to analyze the threshold gains and emission efficiencies of the circular Bragg microdisk lasers [10]. However, such a comprehensive study on the annular Bragg lasers and their transverse modal control is yet to be done. Thus this paper will focus on these subjects.

This paper is organized as follows. In Section 2, we briefly review the comprehensive coupled mode theory derived in [10]. In Section 3, we apply the coupled mode theory to the ABR laser structures and then derive their governing characteristic equation. In Section 4, we first compare the modal threshold gains of two kinds of ABR lasers – one with a $\pi/2$ phase shift in the outer grating and the other without, then find the conditions for a single defect mode lasing. In Section 5 we present a conclusion.

2. Comprehensive coupled mode theory

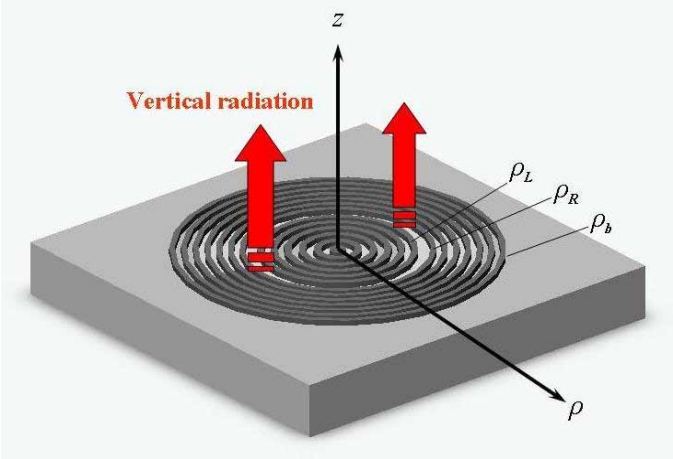

Fig. 1. Illustration of an annular Bragg laser.

#87228 - $15.00 USD Received 5 Sep 2007; revised 1 Nov 2007; accepted 28 Nov 2007; published 10 Dec 2007

As illustrated in Fig. 1, an annular Bragg laser consists of a circumferentially guiding defect and the surrounding annular Bragg gratings in a gain medium. The inner grating spans from the center to ρ_L while the outer grating spans from ρ_R to ρ_b. In the case that the polarization effects due to the waveguide structure are not concerned, we can introduce the "weak guidance approximation," under which all the field components can be obtained from the z component of the electric field which satisfies the scalar wave equation in cylindrical coordinates

$$\left[\frac{1}{\rho}\frac{\partial}{\partial\rho}\left(\rho\frac{\partial}{\partial\rho}\right)+\frac{1}{\rho^2}\frac{\partial^2}{\partial\varphi^2}+k_0^2n^2(\rho,z)+\frac{\partial^2}{\partial z^2}\right]E_z(\rho,\varphi,z)=0, \tag{1}$$

where $k_0=\frac{\omega}{c}=\frac{2\pi}{\lambda_0}$ is the wave number in vacuum. For an azimuthally propagating eigenmode, the E_z in a passive uniform medium in which the dielectric constant $n^2(\rho,z)=\varepsilon_r(z)$ can be expressed as

$$\begin{aligned}E_z(\rho,\varphi,z)&=E_z^{(m)}(\rho,z)\exp(im\varphi)\\&=\left[AH_m^{(1)}(\beta\rho)+BH_m^{(2)}(\beta\rho)\right]Z(z)\exp(im\varphi),\end{aligned} \tag{2}$$

where m is the azimuthal mode number, $\beta = k_0 n_{eff}$ is the in-plane propagation constant, and $Z(z)$ is the fundamental mode profile of the planar slab waveguide satisfying

$$\left(k_0^2\varepsilon_r(z)+\frac{\partial^2}{\partial z^2}\right)Z(z)=\beta^2Z(z). \tag{3}$$

In a radially perturbed gain medium, the dielectric constant can be expressed as $n^2(\rho,z)=\varepsilon_r(z)+i\varepsilon_i(z)+\Delta\varepsilon(\rho,z)$ where $|\varepsilon_i(z)|<<\varepsilon_r(z)$ represents the gain/loss and $\Delta\varepsilon(\rho,z)$ reflects the contribution of perturbation. For optimal field confinement the perturbation $\Delta\varepsilon(\rho,z)$ has to be expanded in Hankel-phased plane wave series [8]

$$\begin{aligned}\Delta\varepsilon(\rho,z)&=-\Delta\varepsilon_0\sum_{l=\pm1,\pm2}a_l(z)\exp\left(-il\Phi[H_m^{(1)}(\beta_{design}\rho)]\right)\\&=-\Delta\varepsilon_0\sum_{l=\pm1,\pm2}a_l(z)\exp\left(-il\Phi[H_m^{(1)}(x)]\right)\exp(-il\delta\cdot x)\\&=-\Delta\varepsilon_0\left(a_2(z)\frac{H_m^{(2)}}{H_m^{(1)}}e^{-2i\delta\cdot x}+a_{-2}(z)\frac{H_m^{(1)}}{H_m^{(2)}}e^{2i\delta\cdot x}+a_1(z)\frac{H_m^{(2)}}{\left|H_m^{(1)}\right|}e^{-i\delta\cdot x}+a_{-1}(z)\frac{H_m^{(1)}}{\left|H_m^{(1)}\right|}e^{i\delta\cdot x}\right),\end{aligned} \tag{4}$$

In the above expression, $a_l(z)$ is the expansion coefficient of $\Delta\varepsilon(\rho,z)$ at a given z. x is the normalized radius defined as $x=\beta\rho$. $\delta=(\beta_{\text{design}}-\beta)/\beta$ ($|\delta|<<1$), the normalized frequency detuning factor, represents the relative frequency shift from the optimal coupling design.

To account for the vertically radiating fields, we include an additional term $\Delta E(x,z)$ so that

$$E_z^{(m)}(x,z)=\left[A(x)H_m^{(1)}(x)+B(x)H_m^{(2)}(x)\right]Z(z)+\Delta E(x,z). \tag{5}$$

Assuming that the radiating field $\Delta E(x,z)$ has an $\exp(\pm ik_0z)$ dependence on z in free space, i.e.

$$\left[\frac{1}{\rho}\frac{\partial}{\partial\rho}\left(\rho\frac{\partial}{\partial\rho}\right)-\frac{m^2}{\rho^2}\right]\Delta E=0, \tag{6}$$

substituting (4), (5), (6) into (1), introducing the large-radius approximations [8]

$$\frac{H_m^{(1,2)}(x)}{x}\ll\frac{dH_m^{(1,2)}(x)}{dx},\ \frac{d^nH_m^{(1,2)}(x)}{dx^n}\approx(\pm i)^nH_m^{(1,2)}(x), \tag{7}$$

neglecting the second derivatives of $A(x)$ and $B(x)$, and applying the modal solution in the passive unperturbed case, we find

#87228 - $15.00 USD Received 5 Sep 2007; revised 1 Nov 2007; accepted 28 Nov 2007; published 10 Dec 2007

$$
\begin{aligned}
&2iZ\left(\frac{dA}{dx}H_m^{(1)}-\frac{dB}{dx}H_m^{(2)}\right)+i\frac{k_0^2\varepsilon_i}{\beta^2}\left(AH_m^{(1)}Z+BH_m^{(2)}Z\right)+\frac{1}{\beta^2}\left(k_0^2\varepsilon_r+ik_0^2\varepsilon_i+\frac{\partial^2}{\partial z^2}\right)\Delta E\\
&=\frac{k_0^2\Delta\varepsilon_0}{\beta^2}\left(a_2\frac{H_m^{(2)}}{H_m^{(1)}}e^{-2i\delta\cdot x}+a_{-2}\frac{H_m^{(1)}}{H_m^{(2)}}e^{2i\delta\cdot x}\right.\\
&\qquad\left.+a_1\frac{H_m^{(2)}}{\left|H_m^{(1)}\right|}e^{-i\delta\cdot x}+a_{-1}\frac{H_m^{(1)}}{\left|H_m^{(1)}\right|}e^{i\delta\cdot x}\right)\left(AH_m^{(1)}Z+BH_m^{(2)}Z+\Delta E\right).
\end{aligned}
\tag{8}
$$

The phase-matching condition requires that the source and wave have close phase dependence. Grouping the terms with the same kind of Hankel functions leads to the following set of coupled equations

$$
\begin{cases}
2i\dfrac{dA}{dx}H_m^{(1)}Z+i\dfrac{k_0^2\varepsilon_i}{\beta^2}AH_m^{(1)}Z=\dfrac{k_0^2\Delta\varepsilon_0}{\beta^2}\left(a_{-2}BH_m^{(1)}e^{2i\delta\cdot x}Z+a_{-1}\dfrac{\Delta E}{\left|H_m^{(1)}\right|}H_m^{(1)}e^{i\delta\cdot x}\right) & (a)\\
-2i\dfrac{dB}{dx}H_m^{(2)}Z+i\dfrac{k_0^2\varepsilon_i}{\beta^2}BH_m^{(2)}Z=\dfrac{k_0^2\Delta\varepsilon_0}{\beta^2}\left(a_2AH_m^{(2)}e^{-2i\delta\cdot x}Z+a_1\dfrac{\Delta E}{\left|H_m^{(1)}\right|}H_m^{(2)}e^{-i\delta\cdot x}\right) & (b)\\
\left(k_0^2\varepsilon_r+\dfrac{\partial^2}{\partial z^2}\right)\Delta E=k_0^2\Delta\varepsilon_0\left(a_1A\left|H_m^{(1)}\right|e^{-i\delta\cdot x}Z+a_{-1}B\left|H_m^{(1)}\right|e^{i\delta\cdot x}Z\right) & (c)
\end{cases}
\tag{9}
$$

From (9c), ΔE can be expressed as

$$
\Delta E=\left(s_1Ae^{-i\delta\cdot x}+s_{-1}Be^{i\delta\cdot x}\right)\left|H_m^{(1)}\right|,
\tag{10}
$$

where

$$
s_l(z)=k_0^2\Delta\varepsilon_0\int_{-\infty}^{+\infty}a_l(z')Z(z')G(z,z')dz',
\tag{11}
$$

and $G(z,z')$ is the Green's function satisfying $\left(k_0^2\varepsilon_r(z)+\dfrac{\partial^2}{\partial z^2}\right)G(z,z')=\delta(z-z').$

Substituting (10) into (9a) and (9b), multiplying both sides by $Z(z)$ and integrating over z, we arrive at

$$
\begin{cases}
\dfrac{dA}{dx}=\left(g_A-h_{-1,1}\right)A-\left(h_{-1,-1}+ih_2\right)Be^{2i\delta\cdot x}\\
\dfrac{dB}{dx}=-\left(g_A-h_{1,-1}\right)B+\left(h_{1,1}+ih_2\right)Ae^{-2i\delta\cdot x},
\end{cases}
\tag{12}
$$

where the gain coefficient $g_A\equiv-\dfrac{k_0^2}{2P\beta^2}\int_{-\infty}^{+\infty}\varepsilon_i(z)Z^2(z)dz,$ the radiation coupling coefficients $h_{\pm1,\pm1}=\dfrac{ik_0^2\Delta\varepsilon_0}{2P\beta^2}\int_{-\infty}^{+\infty}a_{\pm1}(z)s_{\pm1}(z)Z(z)dz,$ the feedback coupling coefficient $h_2=h_{\pm2}=\dfrac{k_0^2\Delta\varepsilon_0}{2P\beta^2}\int_{-\infty}^{+\infty}a_{\pm2}(z)Z^2(z)dz,$ and the normalization constant $P\equiv\int_{-\infty}^{+\infty}Z^2(z)dz.$

In the case of index grating, we can choose the phase of the grating such that $a_{-1}=a_1$, then all the radiation coupling coefficients are the same and can be denoted as h_1. Let $u=g_A-h_1$ and $v=h_1+ih_2$, then the generic solution to (12) is

#87228 - $15.00 USD Received 5 Sep 2007; revised 1 Nov 2007; accepted 28 Nov 2007; published 10 Dec 2007

$$\begin{cases} A(x) = \left[C_1 \exp(Sx) + C_2 \exp(-Sx)\right] \exp(i\delta \cdot x) \\ B(x) = -\dfrac{1}{v}\left[C_1 (S - u + i\delta) \exp(Sx) - C_2 (S + u - i\delta) \exp(-Sx)\right] \exp(-i\delta \cdot x), \end{cases} \tag{13}$$

where $S \equiv \sqrt{(u - i\delta)^2 - v^2}$. In analogy to the case of a linear grating [11], the modes with a real *S* manifest themselves as band-gap modes since they are located within the band gap in the band diagram and their fields are reflected in the grating region. They are mostly confined in the guiding defect so that they are also termed as "defect modes." In the unperturbed region where $\Delta\varepsilon$=0, we have h_1=h_2=0, and the solution to (12) is simply

$$\begin{cases} A(x) = A(0) \exp(g_A x) \\ B(x) = B(0) \exp(-g_A x). \end{cases} \tag{14}$$

3. Modal fields and characteristic equation of annular Bragg lasers

For an ABR laser as shown in Fig. 1, the electric field $E_z^{(m)}(x, z)$ in different regions takes different forms

$$E_z^{(m)}(x, z) = \begin{cases} A_1(x) H_m^{(1)}(x) Z(z) + B_1(x) H_m^{(2)}(x) Z(z) + \Delta E_1(x, z), & \textit{region I}: \ x < x_L \\ A_2 e^{g_A x} H_m^{(1)}(x) Z(z) + B_2 e^{-g_A x} H_m^{(2)}(x) Z(z), & \textit{region II}: \ x_L < x < x_R \\ A_3(x) H_m^{(1)}(x) Z(z) + B_3(x) H_m^{(2)}(x) Z(z) + \Delta E_3(x, z), & \textit{region III}: x_R < x < x_b. \end{cases} \tag{15}$$

where x_L, x_R, and x_b are normalized ρ_L, ρ_R, and ρ_b, respectively.

Designed in a passive model, the demonstrated ABR lasers in [9] introduced a $\pi/2$ phase shift in their outer gratings. This, however, as will be discussed later, is unfavorable for single defect mode operation. Therefore, we will study two cases: (1) the outer grating (region III) has an additional $\pi/2$ phase shift compared to the inner grating (region I); (2) both the inner grating and the outer grating have the same phase dependence $\Phi[H_m^{(1)}(x)]$. So in case (1), we need to change a_1 to ia_1, a_{-1} to $-ia_{-1}$, and a_2 to $-a_2$ in region III. From their definitions, $h_{1,1}$, $h_{-1,-1}$ and h_2 have a sign flip while $h_{1,-1}$ and $h_{-1,1}$ keep the same, which means that the additional phase shift doesn't have an effect on the vertical radiation mechanism. Thus in region III, A_3 and B_3 can still be expressible as (13) provided that we replace *v* by $v' = -v$. For the same reason, the radiation field $\Delta E_3 = \left(s_1' A e^{-i\delta \cdot x} + s_{-1}' B e^{i\delta \cdot x}\right) \left| H_m^{(1)} \right|$ where $s_1' = is_1$ and $s_{-1}' = -is_{-1}$.

We invoke the following boundary conditions for TE modes:

(1) At the center x = 0, the total amplitude must remain finite and it should be satisfied at any *z*. Since in region I, $E(x, z) = A_1(x) H_m^{(1)}(x) Z(z) + B_1(x) H_m^{(2)}(x) Z(z) + \Delta E_1(x, z)$ and $\left|\Delta E_1(x, z)\right| \ll \left|A_1(x) H_m^{(1)}(x) Z(z) + B_1(x) H_m^{(2)}(x) Z(z)\right|$, we can set $A_1(0) = B_1(0)$.

(2) At the exterior boundary x_b, no incoming wave comes from outside ($x > x_b$), thus $B_3(x_b) = 0$.

(3) At the interfaces x_L and x_R, the electric field E_z is continuous, i.e., $E_I(x_L) = E_{II}(x_L)$ and $E_{II}(x_R) = E_{III}(x_R)$.

(4) At the interfaces x_L and x_R, the first order derivative of the electric field E_z' is continuous, i.e., $E_I'(x_L) = E_{II}'(x_L)$ and $E_{II}'(x_R) = E_{III}'(x_R)$.

By matching the boundary conditions (1) and (2), then multiplying by $Z(z)$ and integrating over *z*, we get the integrated $E_z^{(m)}(x)$ in the 3 different regions:

#87228 - $15.00 USD Received 5 Sep 2007; revised 1 Nov 2007; accepted 28 Nov 2007; published 10 Dec 2007

$$
\begin{cases}
E_I(x) = PC_{11}\left[e^{S\cdot x+i\delta\cdot x} + \dfrac{S-u+v+i\delta}{S+u-v-i\delta} e^{-S\cdot x+i\delta\cdot x} \right] H_m^{(1)}(x) \\
\qquad\qquad -\dfrac{PC_{11}}{v}\left[(S-u+i\delta)e^{S\cdot x-i\delta\cdot x} - \dfrac{S-u+v+i\delta}{S+u-v-i\delta}(S+u-i\delta)e^{-S\cdot x-i\delta\cdot x} \right] H_m^{(2)}(x) \\
E_{II}(x) = P\left[A_2 e^{g_A x} H_m^{(1)}(x) + B_2 e^{-g_A x} H_m^{(2)}(x) \right] \\
E_{III}(x) = PC_{31} e^{S\cdot x+i\delta\cdot x}\left[1+\dfrac{S-u+i\delta}{S+u-i\delta} e^{2S(x_b-x)} \right] H_m^{(1)}(x) \\
\qquad\qquad -\dfrac{PC_{31}(S-u+i\delta)}{v'} e^{S\cdot x-i\delta\cdot x}\left[1-e^{2S(x_b-x)} \right] H_m^{(2)}(x),
\end{cases}
\tag{16}
$$

where P is the normalization constant defined before. By satisfying the boundary conditions (3) and (4), we finally arrive at the characteristic equation for the annular Bragg lasers:

$$
\frac{(g_A+i)(LHS)_I - 1}{(g_A+i)(LHS)_I + 1} \cdot \frac{(g_A+i)(RHS)_{III} + 1}{(g_A+i)(RHS)_{III} - 1} = e^{2g_A(x_R-x_L)} \frac{H_m^{(1)}(x_R)}{H_m^{(2)}(x_R)} \cdot \frac{H_m^{(2)}(x_L)}{H_m^{(1)}(x_L)}, \tag{17}
$$

where

$$
(LHS)_I = \frac{\begin{Bmatrix} \left[e^{S\cdot x_L+i\delta\cdot x_L} + \dfrac{S-u+v+i\delta}{S+u-v-i\delta} e^{-S\cdot x_L+i\delta\cdot x_L} \right] H_m^{(1)}(x_L) \\ -\dfrac{1}{v}\left[(S-u+i\delta)e^{S\cdot x_L-i\delta\cdot x_L} - \dfrac{S-u+v+i\delta}{S+u-v-i\delta}(S+u-i\delta)e^{-S\cdot x_L-i\delta\cdot x_L} \right] H_m^{(2)}(x_L) \end{Bmatrix}}{\begin{Bmatrix} \left[\big(S+i(\delta+1)\big)e^{S\cdot x_L+i\delta\cdot x_L} + \dfrac{S-u+v+i\delta}{S+u-v-i\delta}\big(-S+i(\delta+1)\big)e^{-S\cdot x_L+i\delta\cdot x_L} \right] H_m^{(1)}(x_L) \\ -\dfrac{1}{v}\left[(S-u+i\delta)\big(S-i(\delta+1)\big)e^{S\cdot x_L-i\delta\cdot x_L} + \dfrac{S-u+v+i\delta}{S+u-v-i\delta}(S+u-i\delta)\big(S+i(\delta+1)\big)e^{-S\cdot x_L-i\delta\cdot x_L} \right] H_m^{(2)}(x_L) \end{Bmatrix}}
$$

and

$$
(RHS)_{III} = \frac{\begin{matrix} e^{S\cdot x_R+i\delta\cdot x_R}\left[1+\dfrac{S-u+i\delta}{S+u-i\delta} e^{2S(x_b-x_R)} \right] H_m^{(1)}(x_R) - \dfrac{(S-u+i\delta)}{v'} e^{S\cdot x_R-i\delta\cdot x_R}\left[1-e^{2S(x_b-x_R)} \right] H_m^{(2)}(x_R) \end{matrix}}{\begin{Bmatrix} \big(S+i(\delta+1)\big)e^{S\cdot x_R+i\delta\cdot x_R}\left[1+\dfrac{S-u+i\delta}{S+u-i\delta} e^{2S(x_b-x_R)} \right] H_m^{(1)}(x_R) - 2S\dfrac{S-u+i\delta}{S+u-i\delta} e^{S\cdot x_R+i\delta\cdot x_R} e^{2S(x_b-x_R)} H_m^{(1)}(x_R) \\ -\dfrac{(S-u+i\delta)}{v'}\big(S-i(\delta+1)\big)e^{S\cdot x_R-i\delta\cdot x_R}\left[1-e^{2S(x_b-x_R)} \right] H_m^{(2)}(x_R) - 2S\dfrac{(S-u+i\delta)}{v'} e^{S\cdot x_R-i\delta\cdot x_R} e^{2S(x_b-x_R)} H_m^{(2)}(x_R) \end{Bmatrix}}.
$$

4. Numerical results and modal control in annular Bragg lasers

Without loss of generality, we assume an annular Bragg laser fabricated in a layer structure as described in [12] which was designed for 1.55-μm laser emission. We approximate the complicated layer structure by an effective index profile comprising five layers: lower cladding, n=1.54; first layer, n=3.281 and thickness of 60.5 nm; second layer (the active region), n=3.4057 and thickness of 129 nm; third layer, n=3.281 and thickness of 60.5 nm; upper cladding, n=1.54. Numerical calculations of the mode profile and the effective index of the approximated layer structure indicate negligible deviations from those of the exact one. Here we focus our analysis on the case of a shallow grating with an etch depth of ~185 nm. The vertical mode profile $Z(z)$, the effective index n_{eff}, and the Green's function are

#87228 - $15.00 USD Received 5 Sep 2007; revised 1 Nov 2007; accepted 28 Nov 2007; published 10 Dec 2007

numerically calculated. For the in-plane grating, we assume a rectangular profile with a Hankel-phased modulation [8] $\Theta(\Phi[H_m^{(1)}(x)],\alpha)=\begin{cases}1, & \cos\left(\Phi[H_m^{(1)}(x)]\right)\ge\alpha\\ 0, & \cos\left(\Phi[H_m^{(1)}(x)]\right)<\alpha\end{cases}$, which can be expanded in Fourier series as

$$\Theta(\Phi[H_m^{(1)}(x)],\alpha)=\frac{\arccos\alpha}{\pi}+\frac{2}{\pi}\sum_{l=1}^{\infty}\frac{\sin(l\arccos\alpha)}{l}\cos\left(l\Phi[H_m^{(1)}(x)]\right). \tag{18}$$

This yields the expansion coefficients $a_2=a_{-2}=\frac{\sin(2\pi d_c)}{2\pi}$ and $a_1=a_{-1}=\frac{\sin(\pi d_c)}{\pi}$ where $d_c\equiv\frac{\arccos\alpha}{\pi}$ ($-1<\alpha<1$, $0<d_c<1$) is the duty cycle of the Hankel-phase-modulated rectangular grating. We have pointed out in [10] that, to get both strong radiation coupling out of the resonator and in-plane feedback from the grating, d_c=0.25 is a good choice since h_2 is maximal while Re(h_1) is not small. For m=0, we get h_1=0.0072+0.0108i and h_2=0.0601.

It should be noted that we are not trying, also it's unnecessary, to find all the eigenmodes of a given laser structure. We are more concerned about what laser structure can have a low-threshold high-efficiency single mode lasing. In general, larger devices with more Bragg layers can yield modes with lower threshold levels, but they also have smaller mode discrimination, making it harder for mode selection. For calculation, we adopt a typical value for the exterior boundary radius ρ_b=17.5μm ($x_b=\beta\rho_b\approx$200) used in [9]. Also we assume the annular defect is located at the middle x_b/2, with its width (x_R-x_L) being a wavelength of the cylindrical waves therein. So (x_L+x_R)/2=x_b/2, and $x_R-x_L=2\pi\approx$6.3 since the approximation of Hankel functions $H_m^{(1,2)}(x)\approx\sqrt{\frac{2}{\pi x}}\exp\left[\pm i\left(x-\frac{m\pi}{2}-\frac{\pi}{4}\right)\right]$ holds when away from the center. We then put all the parameters x_L, x_R, x_b into (17), solve for all the allowed pairs of g_A and δ, and pick up those within the range $0<g_A<0.01$, $-0.1<\delta<0.1$. Table 1 shows the threshold gains g_A, the detuning factors δ, and the in-plane modal field patterns of the first five resonant modes of the ABR lasers whose outer grating has an additional $\pi/2$ phase shift.

#87228 - $15.00 USD Received 5 Sep 2007; revised 1 Nov 2007; accepted 28 Nov 2007; published 10 Dec 2007

Table 1. Modal threshold gains, detuning factors, and modal field patterns of the ABR lasers (x_b = 200) which have a $\pi/2$ phase shift in the outer grating.

Number	Threshold gain g_A (10^{-3})	Detuning factor δ (10^{-3})	Modal field pattern
1	0.832	66.1	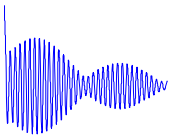
2	1.25	67.5	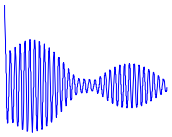
3	2.58	81.5	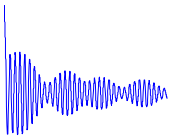
4	3.52	85.9	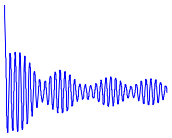
5	5.89	−14.3	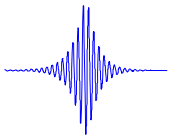

We see that the modes are asymmetrically located with respect to the designed Bragg frequency (δ=0). This is because we are using a mixed-order Bragg grating, and the interference of the radiation due to first-order diffraction breaks the mode degeneracy of in-plane (guided) waves, which was first proposed for longitudinal mode selection in linear DFB lasers [13]. For this reason, actually, there is no need to introduce the $\pi/2$ phase shift in the outer grating. On the other hand, the additional $\pi/2$ phase shift separates the whole resonator into two coupled resonators. This is like a Febry-Perot resonator in which a $\lambda/4$ plate is inserted at the middle point. The difference in the amount of feedback from its two end facets breaks the degeneracy of the eigenmodes of the new structure, as can be seen from a comparison between Mode 1 and 2, and also between Mode 3 and 4. Due to the coupling loss between the two separated resonators, the defect mode whose maximal field is at the middle point has a relatively high g_A, as evidenced by Mode 5. To reduce the threshold gain of the defect mode, we consider the ABR lasers whose outer grating has the same phase dependence $\Phi[H_m^{(1)}(x)]$ as the inner grating. The calculated results are listed in Table 2. As expected, the defect mode now possesses the lowest threshold gain, which is almost an order of magnitude lower than that in the previous case. The higher-order (in-band) modes resemble their counterparts in a non-periodic circular grating DFB laser (in which no defect is introduced in the middle and the Hankel-phased grating spreads from the center to the exterior boundary).

#87228 - $15.00 USD Received 5 Sep 2007; revised 1 Nov 2007; accepted 28 Nov 2007; published 10 Dec 2007

Table 2. Modal threshold gains, detuning factors, and modal field patterns of the ABR lasers (x_b = 200) which have the same phase dependence in the inner and outer gratings.

Number	Threshold gain g_A (10^{-3})	Detuning factor δ (10^{-3})	Modal field pattern
1	0.632	54.9	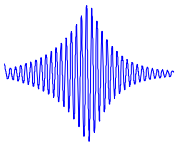
2	1.07	66.9	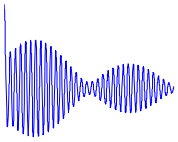
3	1.92	70.9	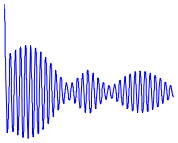
4	3.15	84.4	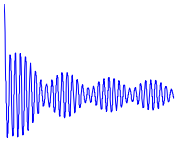
5	4.11	91.1	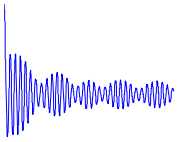

In such grating-coupled surface emitting lasers, the total power loss is composed of two contributions: the coherently scattered, vertically emitted light comprises our useful signal, while the in-plane transverse loss from the resonator is the power leakage [10]. We define the emission efficiency η as the ratio between the useful vertical radiation power and the total power loss. We vary the exterior boundary radius x_b while fixing the defect size and locating the defect always at the middle (x_b/2), and calculate η for both the defect mode and the first in-band mode as a function of x_b. The results are plotted in Fig. 2. As can be seen, the emission efficiency, for both modes, improves as the device size (x_b) increases, and more impressively, the defect mode has much higher emission efficiency than the first in-band mode for the same device size.

#87228 - $15.00 USD Received 5 Sep 2007; revised 1 Nov 2007; accepted 28 Nov 2007; published 10 Dec 2007

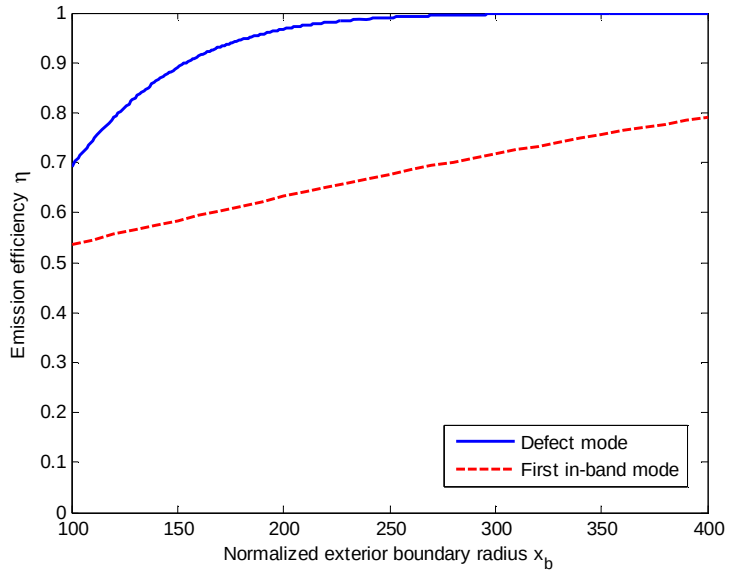

Fig. 2. Emission efficiency η of the defect mode and the first in-band mode, as a function of the normalized exterior boundary radius x_b.

Since larger device size results in smaller threshold gains for in-band modes and smaller modal discrimination, there is an upper limit for the exterior boundary radius x_b for a single defect mode operation. The calculated threshold gain g_A and detuning factor δ as a function of the exterior boundary radius x_b are displayed in Fig. 3. We see that, for x_b>250 (ρ_b>21.8μm), the first in-band mode has a lower threshold gain than the defect mode, so x_b has to be less than 250 to guarantee a single defect mode lasing.

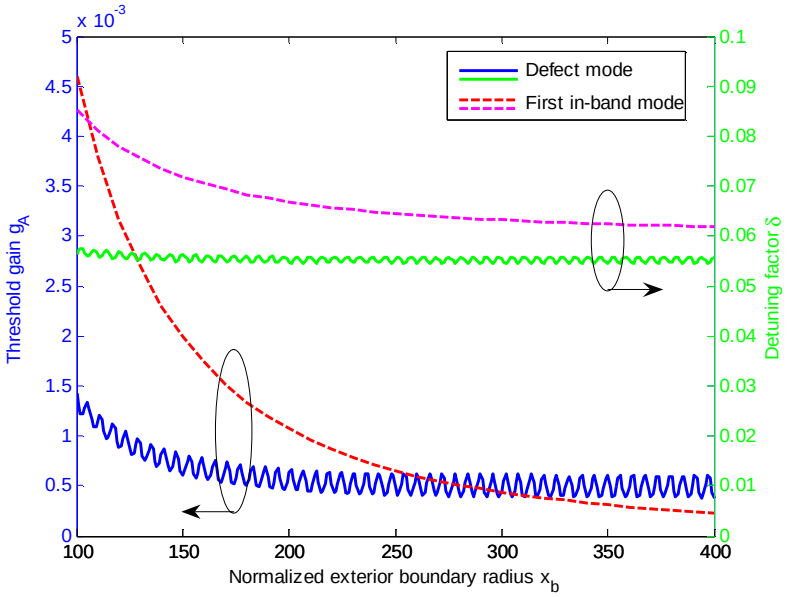

Fig. 3. Threshold gain g_A and detuning factor δ, of the defect mode and the first in-band mode, as a function of the normalized exterior boundary radius x_b.

#87228 - $15.00 USD Received 5 Sep 2007; revised 1 Nov 2007; accepted 28 Nov 2007; published 10 Dec 2007

We also notice the periodic oscillation in g_A and δ. This can be understood by the phase factor in the mode resonance condition. Derived from the solutions to (12), the reflectivity of a eigenwave incident from outward to inward on the interface x_L subject to the boundary condition $A(-x_b/2)=B(-x_b/2)$ is

$$r_1 = e^{-i(\delta+iu)x_b} \frac{\left(ve^{i(\delta+iu)x_b} + i\delta - u\right)\sinh\left(\frac{Sx_b}{2}\right) + S\cosh\left(\frac{Sx_b}{2}\right)}{-\left(ve^{-i(\delta+iu)x_b} + i\delta - u\right)\sinh\left(\frac{Sx_b}{2}\right) + S\cosh\left(\frac{Sx_b}{2}\right)}, \tag{19}$$

while from inward to outward on the interface x_R subject to the boundary condition $B(x_b/2)=0$ is

$$r_2 = \frac{-v\sinh\left(\frac{Sx_b}{2}\right)}{\left(i\delta - u\right)\sinh\left(\frac{Sx_b}{2}\right) + S\cosh\left(\frac{Sx_b}{2}\right)}. \tag{20}$$

The phase difference caused by the interface x_L is

$$\exp\left[-i\Phi\left(\frac{H_m^{(2)}\left(\frac{x_b}{2}\right)}{H_m^{(1)}\left(\frac{x_b}{2}\right)}\right)\right] \approx e^{2i\left(\frac{x_b}{2} - \frac{m\pi}{2} - \frac{\pi}{4}\right)} = -ie^{ix_b}, \tag{21}$$

where m=0 has been assumed. The mode resonance condition requires that $r_1 r_2 \cdot (-ie^{ix_b}) = 1$, thus the phase factor $e^{ix_b}e^{-i\delta x_b} = e^{i(1-\delta)x_b}$ is responsible for the oscillation in g_A and δ.

5. Conclusion

We studied the modal properties and modal control in the ABR lasers. We derived the characteristic equation for such lasers, yielding the modal threshold gains and the resonance frequencies. Two kinds of ABR lasers, one with a $\pi/2$ phase shift in the outer grating and the other without, were analyzed. It was pointed out that the additional $\pi/2$ phase shift in the outer grating actually separates the whole resonator into two, thus raising the threshold gain of the defect mode. We also numerically demonstrated that, in order to get a single high-efficiency defect mode lasing in the ABR lasers, we can choose the kind without a $\pi/2$ phase shift in the outer grating, and also an exterior boundary radius smaller than a critical value.

Acknowledgment

This work was supported in part by the Defense Advanced Research Projects Agency (DARPA) and in part by the National Science Foundation. The authors thank the anonymous reviewers for their helpful comments.

#87228 - $15.00 USD Received 5 Sep 2007; revised 1 Nov 2007; accepted 28 Nov 2007; published 10 Dec 2007